Biochemical and Biophysical Research Communications 525 (2020) 94–99

Contents lists available at ScienceDirect

Biochemical and Biophysical Research Communications

journal homepage: www.elsevier.com/locate/ybbrc

Simultaneous tracking of two motor domains reveals near simultaneous steps and stutter steps of myosin 10 on actin filament bundles

Xianan Qin [a], Hanna Yoo [b, 1], Harry Chun Man Cheng [b, 1], Quang Quan Nguyen [a, 1], Jing Li [a], Xiaoyan Liu [c], Laurence Prunetti [c], Xingxiang Chen [b], Teng Liu [a], H. Lee Sweeney [c, **], Hyokeun Park [a, b, d, *]

[a] Department of Physics, The Hong Kong University of Science and Technology, Clearwater Bay, Kowloon, Hong Kong
[b] Division of Life Science, The Hong Kong University of Science and Technology, Clearwater Bay, Kowloon, Hong Kong
[c] Department of Pharmacology and Therapeutics and the Myology Institute, University of Florida College of Medicine, Gainesville, FL, 32610, USA
[d] State Key Laboratory of Molecular Neuroscience, The Hong Kong University of Science and Technology, Clearwater Bay, Kowloon, Hong Kong

ARTICLE INFO

Article history:
Received 3 February 2020
Accepted 6 February 2020
Available online 17 February 2020

Keywords:
Myosin X
Unconventional myosin
Motility
Single-molecule
Stepping mechanism

ABSTRACT

Myosin X (Myo10) has several unique design features including dimerization via an anti-parallel coiled coil and a long lever arm, which allow it to preferentially move on actin bundles. To understand the stepping behavior of single Myo10 on actin bundles, we labeled two heads of Myo10 dimers with different fluorophores. Unlike previously described for myosin V (Myo5) and VI (Myo6), which display alternating hand-over-hand stepping, Myo10 frequently took near simultaneous steps of both heads, and less frequently, 2–3 steps of one head before the other head stepped. We suggest that this behavior results from the unusual kinetic features of Myo10, in conjunction with the structural properties of the motor domain/lever arm, which will favor movement on actin bundles rather than on single filaments.

1. Introduction

The myosin superfamily of molecular motors provides a large number of functions that involve movement on actin filaments in cells, including cytokinesis, intracellular organelle movements, powering muscle contraction, movement of cells themselves, and other functions [1–5]. There are at least 79 classes of myosin within the myosin superfamily [3] that follow a basic blueprint of a N-terminal motor and a C-terminal targeting (cargo-binding) domain. In dimer-forming myosins, the C-terminal targeting domain is preceded by a coiled coil. The motor domain ends with the converter subdomain, which amplifies rearrangements in the motor and is the first component of the myosin lever arm. The lever arm contains a variable number of CaM/light chain binding sites and additional extensions are found in some myosin classes.

A number of dimeric myosins can move processively on actin, taking hand-over-hand steps, including Class V (Myo5), Class VI (Myo6), and Class X (Myo10), but with different stepping behaviors [6,7]. What is quite different among these myosins is the design of their “lever arms”, which are extensions from the motor domain that amplify changes in the motor conformation to produce a powerstroke on actin. Unlike the lever arm of Myo5, the lever arm of Myo10 is made up of a combination of IQ motifs with associated light chains and a stable, single alpha-helical (SAH) domain.

Myo10 is involved in the formation of and trafficking in filopodia [1]. The formation of filopodia was reported to be induced by the dimerization of Myo10 [8]. There has been controversy as to whether Myo10 preferentially traffics on actin bundles, and if so, what the nature of the stepping behavior is [6,7,9,10]. This was the result of Myo10 having an anti-parallel coiled coil, unlike other myosin classes [11,12]. Proper dimerization is important for normal function of Myo10, allowing its movement to the tips of filopodia and its proper localization in cells [8,11,13]. However, the stepping

* Corresponding author. Department of Physics and Division of Life Science, The Hong Kong University of Science and Technology, Clearwater Bay, Kowloon, Hong Kong.
** Corresponding author. Department of Pharmacology and Therapeutics and the Myology Institute, University of Florida College of Medicine, PO Box 100267, Gainesville, FL, 32610-0267, USA.
E-mail addresses: Lsweeney@ufl.edu (H.L. Sweeney), hkpark@ust.hk (H. Park).
[1] H.Y., H.C.M.C. and Q.Q.N. contributed equally to this work.

https://doi.org/10.1016/j.bbrc.2020.02.039
0006-291X/

mechanism of Myo10 containing the anti-parallel coiled coil is not clearly understood. Herein, we performed *in vitro* single-molecule motility assay of Myo10 using two-color tracking of two heads of Myo10 that allowed us to independently follow the positions of both heads of Myo10 dimers during stepping on actin bundles.

2. Materials and methods

2.1. Myo10 constructs, expression, purification, and labelling

Full-length human Myo10 was constructed with either mApple (red fluorescence protein) or a HaloTag added to the N-terminus, which were preceded by an N-terminal Flag tag. These constructs were used to create recombinant baculoviruses for expression in SF9 cells [12], similar to the previously described method for Myo5 [14]. The virus coding for mApple was co-infected with the virus coding for HaloTag at a ratio of 1:1 in SF9 cells. Three days after infection with these constructs, SF9 cells were lysed in a high ionic strength buffer containing ATP, DTT, Nonidet P-40, and protease inhibitors. Myo10 was purified using an anti-Flag antibody affinity column. Purified proteins were concentrated and stored in a buffer containing (in mM): 75 KCl, 5 Imidazole, 1 DTT, 0.1 $MgCl_2$, 0.025 ADP, 0.5 EGTA and 50% Glycerol (pH adjusted to 7.60). Alexa Fluor 488 (Alexa 488) HaloTag ligand (G1001, Promega) was conjugated to the HaloTag fused to the N-terminus of these purified Myo10 with mApple and HaloTag, following the manufacturer's protocol using a buffer containing (in mM): 20 HEPES, 2 $MgCl_2$, 25 KCl, 1 EGTA and 0.05 ATP (pH adjusted to 7.60).

2.2. Fascin-bundled actin filaments

Actin was purified from rabbit skeletal muscle as described in the previous literature [14]. Fascin was expressed in *E. Coli* and purified as previously described [15]. F-actin and Fascin-bundled actin filaments were prepared as previously described [10]. F-actin filaments were made without 10% biotin-labeled G-actin. F-actin bundles were made by mixing and incubating 3 μM fascin and 8 μM F-actin on ice and stored at 4 °C for two days before use.

2.3. Total internal reflection fluorescence microscope

All fluorescence images were taken using an EMCCD (iXon Ultra, Andor) on an inverted fluorescence microscope (IX73, Olympus) with an oil-immersion 100X objective with a numerical aperture (NA) = 1.49 (UAPON, Olympus). A 15X beam expander (Edmond Optics) and focus lens were used to illuminate the sample uniformly. A laser beam was focused at the back focal plane of an objective lens. An objective-type total internal reflection was generated by making the incidence angle of light greater than the critical angle using a focus lens. Myo10 labeled with Alexa 488 HaloTag and mApple were excited by a 488 nm (Coherent Inc.) and a 561 nm solid state laser (Coherent Inc.), respectively, for SHREC experiments. Both lasers were aligned to the same beam pathway. A dichroic mirror (ZT488/561rpc, Chroma) and an emission filter (ZET488/561 m, Chroma) were used to acquire fluorescence signals from Alexa 488 and mApple. These emission signals of Alexa 488 and mApple were divided into two spectrally distinct channels using a dichroic mirror (T535lpxr, Chroma) in a custom-made dual-view imaging system [16]. An emission filter (ET595/50 m, Chroma) was used in the dual-view to capture the fluorescence of mApple and reduce crosstalk.

2.4. Single-molecule motility assays of Myo10

Sample chambers were prepared as previously described [17,18]. The motility assays of single Myo10 were conducted at room temperature using the motility buffer containing (in mM): 20 HEPES, 25 KCl, 2 $MgCl_2$, 10 DTT, 1 EGTA and 6.25 Calmodulin (pH adjusted to 7.60), as previously described with some modification [6,7,12,19]. NEM myosin with the final concentration of 0.20 mg/mL was added into a sample chamber. After incubation and washing, actin bundles were added. After another incubation and washing, highly concentrated (~1 μM) labeled full-length Myo10 was diluted to a final concentration of ~60 nM and added in the absence of ATP. 2 mM or 2 μM ATP was added before taking images to measure run length or step sizes.

2.5. Measurement of distances between two motor domains of Myo10 using SHREC

SHREC experiments were performed as previously described [20]. To generate a mapping, images of TetraSpeck beads (Thermo Fisher) were collected as previously described [21]. A mapping was generated using collected bead images using the previously reported program codes [22]. The mapping was used to map the location of fluorescent molecules in the Alexa 488 channel onto the mApple channel to confirm the correct mapping of bead images (Fig. S3B) and to calculate the distances of two motor domains of Myo10 labeled with mApple and Alexa 488. The point spread functions of single molecules were fitted into a two dimensional Gaussian to localize their centroids [23,24]. Steps were determined based on a MATLAB program (developed in Ahmet Yildiz's lab at University of California, Berkeley). After the steps were detected, step sizes were calculated as the displacements between neighbored averaged positions. The distances were calculated as Euclidean distances between two positions of two motor domains of Myo10. The multipeak Gaussian fitting to histograms of step sizes or intermotor distances were performed using the normalMixEM procedure of the mixtool package, a multipeak fitting tool programmed by R language [12,25].

3. Results

3.1. Labeling two heads of full-length Myo10 with different fluorophores

To label both heads of full-length Myo10 dimers with two fluorophores, we generated two constructs for Myo10. One construct contained HaloTag fused to the N-terminus of full-length Myo10 (Fig. 1A), and the other construct contained mApple (red fluorescence protein) at the N-terminus(Fig. 1A), which we previously generated and characterized [12]. To promote hetero-dimerization of full-length Myo10 labeled with mApple and a HaloTag conjugated with Alexa 488 (as depicted in Fig. 1B), expressed protein containing both labels was loaded onto fascin-bundled actin filaments (actin bundles) in the absence of nucleotide to induce dimerization (as previously done for full-length Myo6 [19]). ATP was then added to initiate movement. Approximately 60% of fluorescent spots colocalized in both the mApple and Alexa 488 channels, and approximately half of those colocalized spots moved.

3.2. Stepping mechanism of full-length Myo10

Single-molecule motility assay was performed using high concentration of full-length Myo10 labeled with mApple and Alexa 488 on actin bundles. The fluorescence signals of mApple and Alexa 488 were transmitted through two separate light paths and imaged in an EMCCD camera in our custom-made dual-view imaging system. The image of actin bundles decorated with Myo10 labeled with mApple and Alexa 488 is shown in Fig. S1A. The addition of 2 mM

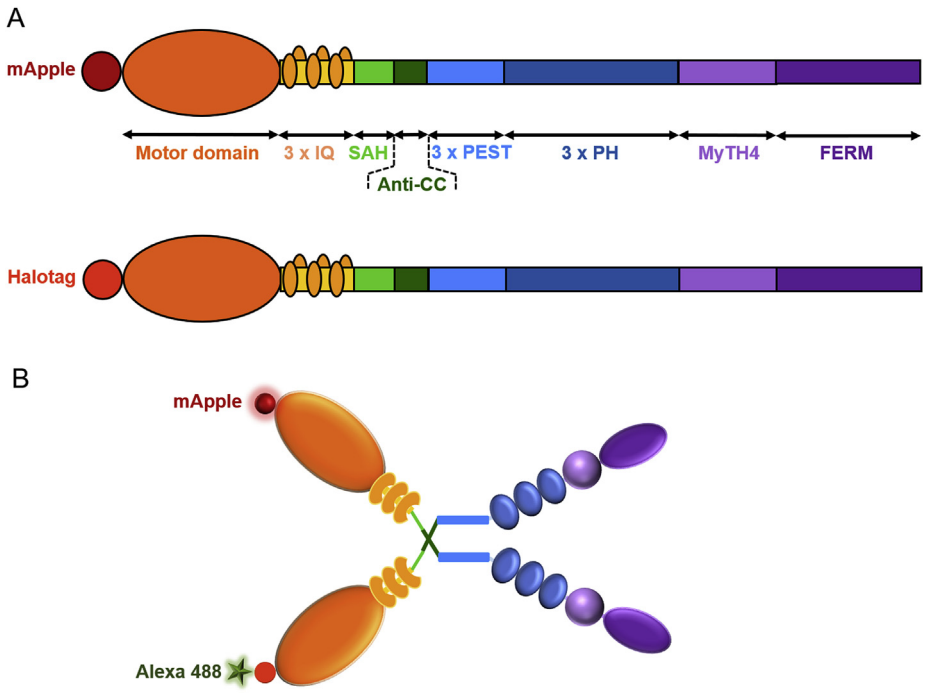

Fig. 1. Diagram of full-length Myo10 with mApple and HaloTag. *A*, The construct of full-length Myo10 with mApple or HaloTag in the N-terminus. *B*, Diagram of full-length Myo10 dimer with mApple and HaloTag labeled with Alexa 488 HaloTag ligand.

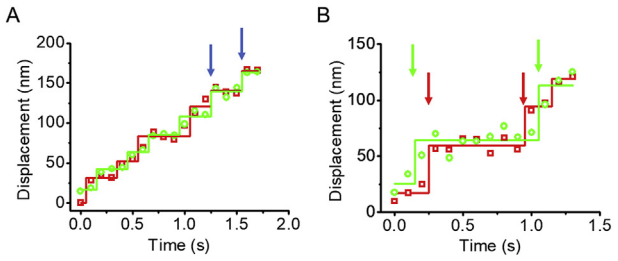

Fig. 2. Stepping of full-length Myo10 moving along actin bundles. *A*, Time trajectories of two heads of a Myo10 showing near simultaneous stepping marked by blue arrows. Two heads alternated with each other in majority of steps, indicating that Myo10 take steps by a hand-over-hand mechanism. *B*, Time trajectories of Myo10 showing multiple steps of one head (marked by red arrows) before the other head takes a step (marked by green arrows). While one motor head labeled with Alexa 488 remained still from 0.2 s to 1.0 s, the other head labeled with mApple took two steps at 0.3 s and 0.9 s. (For interpretation of the references to color in this figure legend, the reader is referred to the Web version of this article.)

ATP caused some full-length Myo10 to move processively with average run-length of 660 ± 54.4 (±SEM) nm (n = 41 (N = 4 experiments) and average velocity of 352 ± 66.0 (n = 41) nm/s whereas the addition of ATP caused other Myo10 to detach from actin bundles.

To understand the detailed stepping mechanism of Myo10 on actin bundles, 2 μM ATP was added into sample chambers. While Myo10 dimers moved on actin bundles processively (Fig. S1B), only data from the two-colored dimers were used. For most of the observed steps, the two heads alternated with each other (Fig. 2*A*), indicating that Myo10 takes steps by a hand-over-hand mechanism as previously reported [10]. Surprisingly, we frequently observed near simultaneous steps, as noted at 1.3 and 1.6 s in Fig. 2*A* (marked by blue arrows). These near simultaneous steps occurred in 49 out of 121 steps (40%) in the mApple labeled head and 49 out of 109 steps (45%) in the Alexa 488-labeled head with 100 ms exposed time. To examine whether these near simultaneous steps can be resolved with higher temporal resolution, we performed the same motility assay with 50 ms exposed time. We still found 6 near simultaneous steps out of 19 steps (32%) in the mApple-labeled head and 6 out of 21 steps (29%) in the Alexa 488-labeled head, implying that near simultaneous stepping is an intrinsic stepping behavior of Myo10. The dwell time distribution of single Myo10 based on the transition of each head shows that zero dwell times are overpopulated as compared to longer dwell times (Fig. S2), further supporting near simultaneous stepping of Myo10. Furthermore, we less frequently observed multiple steps (marked by red arrows in Fig. 2*B*) of one head before the other head stepped. These multiple steps occurred in 15 times in 20 Myo10 molecules and were mainly related to backward steps.

To further investigate the unique stepping mechanism of Myo10, we analyzed the step sizes of two heads labeled with mApple and Alexa 488. The distribution of combined step sizes was broad (Fig. 3*A*), had multiple peaks, and was well fit to a four-Gaussian function using the expectation-maximization algorithm [12,25]. The centers of Gaussian fitting were −49.9, 38.8, 67.7, and 116.9 nm. Recent single-molecule motility assays published on Myo10 reported three peaks of forward center of mass movement of full-length Myo10 (19, 38, and 52 nm) [12] or four peaks of forward center of mass movement of leucine-zippered full-length Myo10 (18, 24, 36, and 54 nm) [26]. Our measured step sizes of Myo10 are roughly twice the reported center of mass of Myo10, supporting that Myo10 takes steps by a hand-over-hand mechanism.

While these multiple peaks of step sizes of Myo10 can be explained by the multiple possible binding sites on actin bundles [27], the inherent flexibility in the Myo10 lever arm and its connections to the motor [12], this distribution includes the near simultaneous steps. The step sizes of the near simultaneous steps (Fig. 3*B*) were larger than those of steps other than near simultaneous steps. Removal of the near simultaneous steps from the distribution of Fig. 3*A* results in the distribution shown in Fig. 3*C*. The distribution with the simultaneous steps removed was still

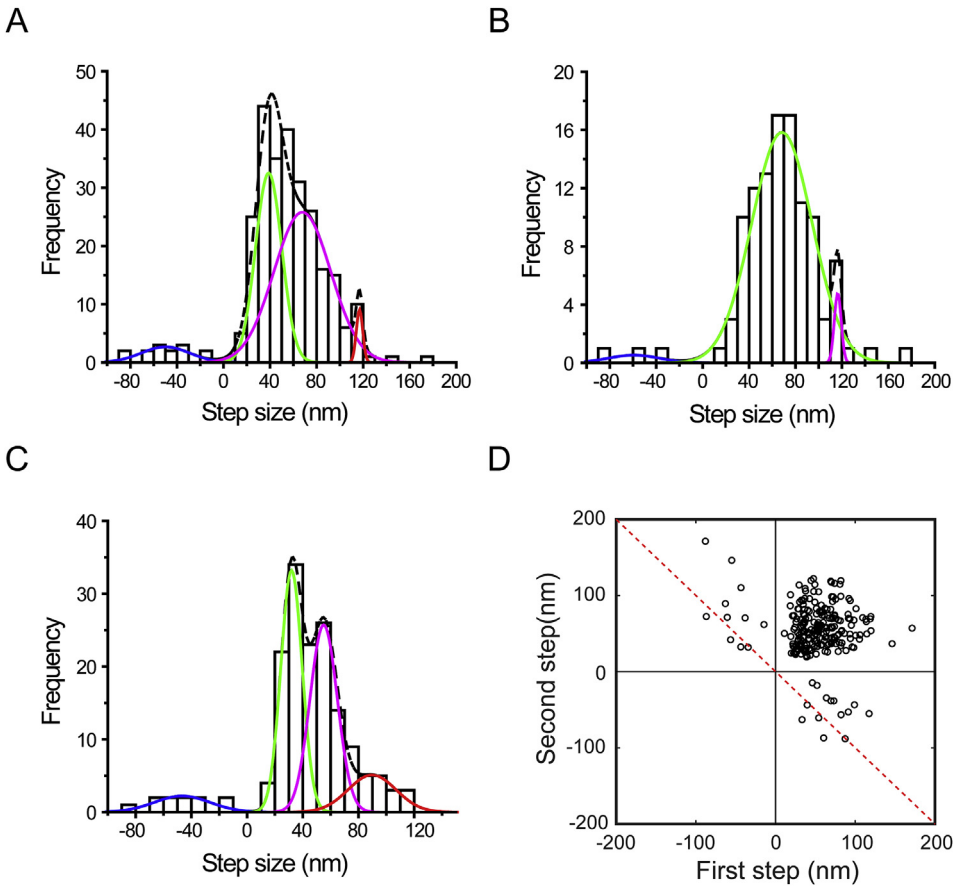

Fig. 3. Step sizes of full-length Myo10. *A,* Histogram of combined step sizes of two heads. The distribution of step sizes (n = 270 steps (N = 9 experiments)) was well fit to a four-Gaussian function (−49.9 ± 20.7 (±SD), 38.8 ± 11.3, 67.7 ± 24.4 and 116.9 ± 2.8 nm). *B,* Histogram of near simultaneous step sizes. The distribution of step sizes (n = 110 steps) was well fit to a three-Gaussian function (−59.3 ± 22.1, 68.3 ± 26.1, and 116.4 ± 3.0 nm). *C,* Histogram of step sizes excluding simultaneous steps. The distribution of step sizes (n = 160 steps) was well fit to a four-Gaussian function (−46.6 ± 20.0, 31.9 ± 7.6, 55.0 ± 9.8 and 89.7 ± 17.1 nm). *D,* Correlation graph between two successive steps. The red dotted line represents the bisector. (For interpretation of the references to color in this figure legend, the reader is referred to the Web version of this article.)

broad, with peaks that are shifted to slightly smaller step sizes. Additionally, the distribution still contains large steps (>70 nm). Thus, many of the largest steps previously reported [12] by tracking center of mass movements were likely derived from near simultaneous steps, given that the previous work had similar temporal resolution to our study.

The prevalence of backward stepping was 5% (14 out of 270 steps (N = 9 experiments), similar to what is observed for Myo6 [28,29]. The distribution of backward step size was broad (Fig. 3A). To find the relationship between backward steps and previous and following steps, we analyzed the correlation between two successive steps of Myo10 as performed for Myo6 [29]. The correlation between two successive steps indicates unique backward stepping patterns of Myo10 (Fig. 3D). Firstly, Myo10 did not take any two successive backward steps. Secondly, the step sizes of most backward step (−49.5 ± 21.6 (±SD) nm (n = 14)) were smaller than previous steps (69.2 ± 24.1 nm (n = 14)), implying that most Myo10 does not move back to the previous binding sites, but to actin binding sites which are ahead of the previous sites. Finally, the steps following backward steps (81.8 ± 45.0 nm (n = 11)) were larger than the backward steps, implying that Myo10 moves further than the previous binding site on the next step.

3.3. Distance between two heads of full-length Myo10

To examine whether observed multiple peaks of step sizes of Myo10 were supported by the distances between two heads of Myo10, we used single-molecule high-resolution colocalization (SHREC), which measures distances between two chromatically different fluorophores by localizing two fluorophores and registering them [20]. Using the images of fluorescent beads in the channels of Alexa 488 and mApple (Fig. S3A), we localized the centroids of the beads in two channels and generated a mapping file, which was used to map the location of fluorescent molecules in the Alexa 488 channel onto the mApple channel (Fig. S3B). Using SHREC, we calculated the distances between two heads of full-length Myo10. The histogram of distances between two heads of Myo10 (Fig. 4) was broad, similar to that of observed step sizes of Myo10. The distribution of distances had multiple peaks and was well fit to a three-Gaussian function with centers at 9.5, 30.3 and 57.8 nm, which are roughly half of multiple peaks of the observed step sizes of Myo10, supporting a hand-over-hand stepping mechanism of full-length Myo10.

4. Discussion

What was surprising in our results is that Myo10, unlike any processive myosin previously described, frequently takes near simultaneous steps and occasionally one head takes multiple steps, or stutter steps, rather than the normal hand-over-hand stepping. Near simultaneous steps (steps of near zero dwell time) have not been observed for other processive myosins, such as Myo5 and Myo6. Such stepping would be prevented by “gating” of the heads. Gating manifests as a stalling of the powerstroke (lever arm swing)

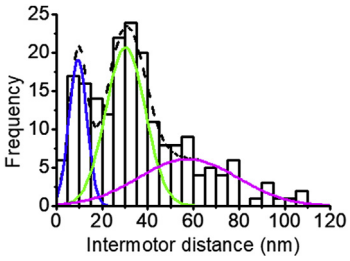

Fig. 4. Intermotor distances of full-length Myo10 using SHREC. Histogram of intermotor distances (n = 194 measurements) was fit to a three-Gaussian function (9.5 ± 3.9, 30.3 ± 8.7 and 57.8 ± 21.6 nm).

of the lead head of a dimer stepping on actin. The stalling occurs due to intramolecular strain between the heads that is not removed until the rear head detaches. Following rear head detachment, completion of the lever arm swing of the former lead provides a forward stepping bias for the recently detached rear head.

The kinetics of Myo10 can explain the existence of the relatively frequent near simultaneous steps. The critical difference in the kinetics between Myo10 and Myo5 (a gated, processive myosin), which likely accounts for the unusual stepping behavior of Myo10 is that the gated transition (ADP release) is slow and rate limiting for the overall cycle in the absence of strain for Myo5, while it is rapid for Myo10. For both myosins this step is gated by intramolecular strain when both heads are attached [32]. In the case of Myo10, the rate limiting transition is the step prior to ADP release, the pyrene-quenching transition [12], which is not gated in processive myosins [32,33]. The near simultaneous steps of Myo10 will occur when a step dwells sufficiently long to allow the lead head to complete its pyrene-quenching transition, but is prevented from releasing ADP by intramolecular strain. Once the rear head detaches, the lead head rapidly releases its ADP and binds ATP and detaches. This results in two steps in rapid succession, which we observe as near simultaneous steps, since the measured ADP release rate of ~60/sec (<20 ms dwell time) [12] exceeds our temporal resolution.

The stutter stepping is more difficult to explain, but may arise as a consequence of a loss of gating when the lead head attaches close to the rear head. The lever arm of Myo10, with its three IQ motifs and SAH domain, is similar to a synthetic lever arm that was introduced by Baboolal et al. [34] into Myo5 that contained two IQ motifs and a SAH domain. The introduction of this lever arm into Myo5 abolished gating. Thus, we propose that when Myo10 takes large steps, the geometry imposed by the anti-parallel coiled coil allows gating, since the lever arms are relatively parallel to the actin filament. However, if the steps are short and the lever arm is more perpendicular to the actin filament (as for Myo5), gating may be lost, giving rise to the stutter steps we observe. When gating is lost, the lead head can detach prior to completion of the pyrene-quenching step of the rear head and thus the lever arm of the rear head has not completed the power stroke to release ADP. In this case, the lever arm of the former rear head may allow the former lead head to either take a step in the rearward direction or forward direction. In the case of backward steps, the intramolecular strain will favor the rear head taking the next step (its second consecutive step). In rare instances, where we see multiple forward steps of the former rear head, there must be two consecutive steps that fail to impose a geometry that allows gating to be re-established.

Declaration of competing interest

The authors declare no conflict of interests.

Acknowledgments

We thank Chun Sum Brian Pang for help with data analysis. This work was supported by grants from the Research Grants Council of Hong Kong (26101117, 16101518, N_HKUST613/17, and A-HKUST603/17 to H.P.) and the Innovation and Technology Commission (ITCPD/17-9 to H.P.). HLS was supported by NIH grant DC009100.

Appendix A. Supplementary data

Supplementary data to this article can be found online at https://doi.org/10.1016/j.bbrc.2020.02.039.

Transparency document

Transparency document related to this article can be found online at https://doi.org/10.1016/j.bbrc.2020.02.039.

References

[1] A.B. Bohil, B.W. Robertson, R.E. Cheney, Myosin-X is a molecular motor that functions in filopodia formation, Proc. Natl. Acad. Sci. U. S. A. 103 (2006) 12411–12416.
[2] O. Sato, et al., Human myosin VIIa is a very slow processive motor protein on various cellular actin structures, J. Biol. Chem. 292 (2017) 10950–10960.
[3] M. Kollmar, S. Muhlhausen, Myosin repertoire expansion coincides with eukaryotic diversification in the Mesoproterozoic era, BMC Evol. Biol. 17 (2017) 211.
[4] H.L. Sweeney, A. Houdusse, Myosin VI rewrites the rules for myosin motors, Cell 141 (2010) 573–582.
[5] H.L. Sweeney, A. Houdusse, Structural and functional insights into the Myosin motor mechanism, Annu. Rev. Biophys. 39 (2010) 539–557.
[6] A. Yildiz, et al., Myosin VI steps via a hand-over-hand mechanism with its lever arm undergoing fluctuations when attached to actin, J. Biol. Chem. 279 (2004) 37223–37226.
[7] A. Yildiz, et al., Myosin V walks hand-over-hand: single fluorophore imaging with 1.5-nm localization, Science 300 (2003) 2061–2065.
[8] H. Tokuo, K. Mabuchi, M. Ikebe, The motor activity of myosin-X promotes actin fiber convergence at the cell periphery to initiate filopodia formation, J. Cell Biol. 179 (2007) 229–238.
[9] S. Nagy, et al., A myosin motor that selects bundled actin for motility, Proc. Natl. Acad. Sci. U. S. A. 105 (2008) 9616–9620.
[10] Y. Sun, et al., Single-molecule stepping and structural dynamics of myosin X, Nat. Struct. Mol. Biol. 17 (2010) 485–491.
[11] Q. Lu, F. Ye, Z. Wei, Z. Wen, M. Zhang, Antiparallel coiled-coil-mediated dimerization of myosin X, Proc. Natl. Acad. Sci. U. S. A. 109 (2012) 17388–17393.
[12] V. Ropars, et al., The myosin X motor is optimized for movement on actin bundles, Nat. Commun. 7 (2016) 12456.
[13] T.M. Watanabe, H. Tokuo, K. Gonda, H. Higuchi, M. Ikebe, Myosin-X induces filopodia by multiple elongation mechanism, J. Biol. Chem. 285 (2010) 19605–19614.
[14] E.M. De La Cruz, A.L. Wells, S.S. Rosenfeld, E.M. Ostap, H.L. Sweeney, The kinetic mechanism of myosin V, Proc. Natl. Acad. Sci. U. S. A. 96 (1999) 13726–13731.
[15] S. Ono, et al., Identification of an actin binding region and a protein kinase C phosphorylation site on human fascin, J. Biol. Chem. 272 (1997) 2527–2533.
[16] H. Park, Y. Li, R.W. Tsien, Influence of synaptic vesicle position on release probability and exocytotic fusion mode, Science 335 (2012) 1362–1366.
[17] H. Park, G.T. Hanson, S.R. Duff, P.R. Selvin, Nanometre localization of single ReAsH molecules, J. Microsc. 216 (2004) 199–205.
[18] P.R. Selvin, et al., In Vitro and in Vivo FIONA and Other Acronyms for Watching Molecular Motors Walk. Single-Molecule Techniques: A Laboratory Manual, Cold Spring Harbor Press, Cold Spring Harbor, NY, 2008, pp. 37–71.
[19] H. Park, et al., Full-length myosin VI dimerizes and moves processively along actin filaments upon monomer clustering, Mol. Cell 21 (2006) 331–336.
[20] L.S. Churchman, Z. Okten, R.S. Rock, J.F. Dawson, J.A. Spudich, Single molecule high-resolution colocalization of Cy3 and Cy5 attached to macromolecules measures intramolecular distances through time, Proc. Natl. Acad. Sci. U. S. A. 102 (2005) 1419–1423.
[21] A. Alsina, et al., Real-time subpixel-accuracy tracking of single mitochondria in neurons reveals heterogeneous mitochondrial motion, Biochem. Biophys. Res. Commun. 493 (2017) 776–782.
[22] L.S. Churchman, J.A. Spudich, Colocalization of fluorescent probes: accurate and precise registration with nanometer resolution, Cold Spring Harb. Protoc. (2012) 141–149, 2012.
[23] H. Park, E. Toprak, P.R. Selvin, Single-molecule fluorescence to study

molecular motors, Q. Rev. Biophys. 40 (2007) 87–111.
[24] P.R. Selvin, et al., Fluorescence imaging with one-nanometer accuracy (FIONA), CSH Protoc. (10) (2007) pdb.top27 (2007).
[25] T. Benaglia, D. Chauveau, D.R. Hunter, D.S. Young, Mixtools: an R package for analyzing mixture models, J. Stat. Software 32 (2009), 06.
[26] O. Sato, et al., Activated full-length myosin-X moves processively on filopodia with large steps toward diverse two-dimensional directions, Sci. Rep. 7 (2017) 44237.
[27] R. Ishikawa, T. Sakamoto, T. Ando, S. Higashi-Fujime, K. Kohama, Polarized actin bundles formed by human fascin-1: their sliding and disassembly on myosin II and myosin V in vitro, J. Neurochem. 87 (2003) 676–685.
[28] J. Menetrey, et al., Processive steps in the reverse direction require uncoupling of the lead head lever arm of myosin VI, Mol. Cell 48 (2012) 75–86.
[29] S. Nishikawa, et al., Switch between large hand-over-hand and small inchworm-like steps in myosin VI, Cell 142 (2010) 879–888.
[32] S.S. Rosenfeld, H.L. Sweeney, A model of myosin V processivity, J. Biol. Chem. 279 (2004) 40100–40111.
[33] H.L. Sweeney, et al., How myosin VI coordinates its heads during processive movement, EMBO J. 26 (2007) 2682–2692.
[34] T.G. Baboolal, et al., The SAH domain extends the functional length of the myosin lever, Proc. Natl. Acad. Sci. U. S. A. 106 (2009) 22193–22198.